BMC Musculoskeletal Disorders

RESEARCH

Open Access

Evaluation of infrapatellar fat pad elasticity in knee osteoarthritis using IVIM-DWI-based virtual MR elastography: repeatability and reproducibility analysis

Hui Tan[1], Qiuju Fan[3], Yong Yu[3], Nan Yu[3], Shaoyu Wang[4] and Shunlin Guo[1,2*]

Abstract

Background Fibrosis of the infrapatellar fat pad (IPFP) leads to changes in its stiffness, which may impact knee osteoarthritis. However, few studies have utilized virtual MR elastography to assess the variations of the IPFP. This study aimed to evaluate the value of intravoxel incoherent motion diffusion weighted imaging (IVIM-DWI)-based virtual MR elastography (vMRE) in the IPFP by assessing the test-retest repeatability, as well as intra- and inter-observer reproducibility.

Methods A total of 71 subjects underwent IVIM-DWI examinations, which were conducted twice with an interval of 30–60 min using an 18-channel knee coil at 3T. Shifted apparent diffusion coefficient (sADC) was calculated from two different sets of b-values (b = 200/800 sec/mm^2 and 200/1500 sec/mm^2) and then converted to IVIM-DWI MRI-based virtual shear modulus (μ_{diff_800} and μ_{diff_1500}). Two readers independently delineated regions of interest (ROI) within the IPFP on the vMRE stiffness map to obtain the mean and standard deviation (SD) values of μ_{diff}. Short-term test-retest repeatability, as well as intra- and inter-observer agreement were assessed using the intra-class correlation coefficient (ICC), the coefficient of variation (CoV), and Bland-Altman limits of agreement (LoA).

Results The mean and SD values of μ_{diff_1500}, along with the mean value of μ_{diff_800} exhibited excellent intra- and inter-observer reproducibility agreement (ICC ≥ 0.90 and CoV ≤ 10%, P< 0.001). The intra- and inter-observer ICCs for the mean values of μ_{diff_800} were 0.917 and 0.901, respectively, while the ICCs for the SD values of μ_{diff_800} were 0.870 and 0.863, with CoV exceeding 10% (P< 0.001). The test-retest repeatability of the average value of μ_{diff_1500} was excellent (ICC = 0.902; CoV = 6.8%) compared to μ_{diff_800} (ICC = 0.877; CoV = 15.3%). Test–retest repeatability of SD for μ_{diff_1500} was good (ICC = 0.803; CoV = 11.5%) in comparison to SD for μ_{diff_800} (ICC = 0.796; CoV = 13.5%).

Conclusions IVIM-DWI-based vMRE demonstrated significant potential as a reliable tool for measuring tissue elasticity in the IPFP, exhibiting higher repeatability for μ_{diff_1500} than for μ_{diff_800}.

Keywords Intravoxel incoherent motion, Diffusion-weighted imaging, Elastography, Osteoarthritis, Infrapatellar fat pad

*Correspondence:
Shunlin Guo
guoshl@lzu.edu.cn

Full list of author information is available at the end of the article

Background

Knee osteoarthritis (KOA) is a prevalent chronic degenerative joint disease that impacts the entire joint tissues, including cartilage, synovium, subchondral bone, ligaments, and the infrapatellar fat pad (IPFP), affecting millions worldwide [1–3]. Risk factors for KOA include advanced age, obesity, prior joint injury, genetic predisposition, and excessive mechanical stress on the joint. Knee pain is the most common symptom of KOA, affecting 36.8–60.7% of individuals, which causes limited physical function and reduces the patients' quality of life [1, 4]. Due to the inability to halt the progression of KOA, current treatments focus on relieving pain and maintaining joint function.

MRI has become increasingly used to evaluate the knee joint in recent years. To date, previous studies have primarily focused on the morphological description or semi-quantitative assessment of the IPFP, including its volume, area, and hyperintense signal intensity [4, 5]. The study by Zhong et al. found that alteration in fat fraction within the IPFP are associated with the severity of OA, Hoffa synovitis, and knee pain [6]. While these studies have provided valuable insights into the morphological changes of the IPFP, there has been limited research on the alterations in IPFP elasticity in KOA. Magnetic resonance elastography (MRE) is an innovative non-invasive technique that enables the evaluation of tissue mechanical properties by measuring tissue elasticity [7, 8]. MRE has been used to identify changes in mechanical properties associated with fibrosis [9]. Despite its potential, MRE necessitates unique equipment, settings, and specialized software for post-processing to produce tissue stiffness maps, which have not yet been integrated into a clinical product and are limiting the widespread adoption of MRE in clinical settings [8, 10].

Intravoxel incoherent motion (IVIM) is a promising approach for quantifying biomechanical and hemodynamic information in tissue [11, 12]. Recently, it has been suggested that tissue shear stiffness can be directly measured using diffusion MRI, a method known as virtual magnetic resonance elastography (vMRE) [13], which could be beneficial for evaluating the IPFP in KOA research. The IPFP, also known as Hoffa's fat pad, is an intraarticular and extra-synovial adipose structure of richly innervated tissue within the knee joint, which considers as part of anatomo-functional unit with synovial membrane [14–16]. The IPFP acts as a cushion between the patellar tendon and anterior tibial plateau, providing stability to the patella during physical activity and safeguarding the knee joint from mechanical harm [3, 5, 17]. Previous research has indicated that the IPFP is susceptible to infiltration by immune cells, which subsequently secrete inflammatory mediators and trigger fibrosis, which could lead to alterations in the mechanical stress within the tissue [18]. IPFP fibrosis is considered an important source of chronic pain in KOA, and pathological manifestations associated with IPFP may lead to changes in elasticity [19]. IVIM-DWI-based vMRE has shown promise in identifying abnormal signals in the IPFP, with the attenuation of these IVIM images influenced by tissue elasticity and the choice of acquisition parameters, particularly the IVIM b value. Previous research has optimized sensitivity to Gaussian and non-Gaussian diffusion in DWI vMRE using b values of 200 and 1500 s/mm^2 [20, 21]. Despite this, the reproducibility and stability of this emerging imaging technique in clinical applications have not yet been fully validated.

Therefore, the purpose of this study was to evaluate the robustness of elasticity values of IVIM DWI-based vMRE in IPFP through assessing short-term test-retest repeatability and intra- and inter-observer reproducibility.

Methods

Data sets

This prospective study was approved by the local Institutional Review Board of the authors' institution (SZFYIEC-YJ-2024-47). All participants provided written informed consent to the protocol before the commencement of the study. A total of 71 patients (40 males, age range: 45 to 72 years, mean age, 58.1 ± 8.9 years) enrolled between November 2023 and March 2024 were analyzed. The inclusion criteria were: (1) clinical diagnosis performed following the standard for KOA by the European League Against Rheumatism [22]; (2) participants > 40 years old. The exclusion criteria included: (1) a history of knee trauma within the last three months, malignant tumor, and treatment with drugs or intra-articular injections within the last six months; (2) a history of knee surgery; (3) continuous intake of medications that may cause arthritis; (4) presence of metal implants or cardiac pacemaker, patient suffering claustrophobia; (5) poor image quality.

MRI protocol

All MRI examinations were conducted using a 3T MR scanner (MAGNETOM Vida, Siemens Healthineers, Erlangen, Germany) equipped with 18-channel knee coils, and the patients were in the feet-first supine position. The MRI protocols included the following sequences: T1-weighted spin-echo sequence: repetition time (TR)/echo time (TE) = 450ms /11ms, slice thickness = 4.0 mm, a field of view (FOV) = 160 mm × 160 mm, refocus flip angle = 120°, and voxel size = 0.5 × 0.5 × 4.0 mm^3; T2-weighted fat-suppressed sequence with TR/TE = 2650ms/41ms, slice thickness = 4.0 mm, FOV = 160 mm × 160 mm, refocus flip angle = 150°, and voxel size = 0.5 × 0.5 × 4.0 mm^3; and the IVIM-DWI sequence was acquired using spectral attenuated

inversion recovery (SPAIR) fat-suppression single-shot echo-planar imaging (ss-EPI) with the following parameters: TR/TE = 3000ms/96ms, slice thickness = 4.0 mm, FOV = 160 mm × 160 mm, and voxel size = 0.8 × 0.8 × 4.0 mm^3, simultaneous multi-slice (SMS) = 2, incorporating 10 b-values of 0, 20, 50, 100, 150, 200, 400, 800,1200, and 1500 s/mm^2. The total scan duration was < 9 min. After the initial first scan, participants were instructed to rest outside the scanning room for approximately 30–60 min before undergoing a second scan utilizing the same IVIM-DWI parameters for test-retest reliability.

MRI data post-processing

The stiffness value of IVIM DWI-based vMRE was determined using custom written software in MATLAB (MATLAB R2016a, MathWorks, MA, USA). Two sets of b values of 200–800 s/mm^2 and 200–1500 s/mm^2 was used to estimate the virtual shear stiffness maps (vMRE maps) and sADC as in previous as follows [13]:

$$\mathrm{sADC}_1\left(\frac{mm^2}{\mathrm{sec}}\right)=\frac{\ln\left(\frac{S_{200}}{S_{800}}\right)}{800-200}$$

$$\mathrm{sADC}_2\left(\frac{mm^2}{\mathrm{sec}}\right)=\frac{\ln\left(\frac{S_{200}}{S_{1500}}\right)}{1500-200}$$

where sADC is shifted ADC; S200, S800, and S1500 are the image signals with a b value of 200, 800, and 1500 s/mm2, respectively. Two sets of IVIM-DWI-based shear modulus (μ_{Diff}) images of the IPFP were generated using the following equation, derived by Le Bihan et al. [13, 23].

$$\mu_{diff}\ (\mathrm{kPa})=\alpha\times\mathrm{sADC}\left(\frac{mm^2}{\mathrm{sec}}\right)+\beta$$

where α and β are the calibration coefficients derived by the previous studies with values of -9.8 and 14.0, respectively.

Image analysis

The IVIM-DWI-based vMRE maps were generated on a voxel-by-voxel basis after the removal of the background signal. All the images were imported into a free, open-source software package (ITK-SNAP; version 3.8.0, http://www.itksnap.org/) for segmenting and labeling.

The observers used T2-weighted fat-suppressed (T2FS) images as a reference, and the regions of interest (ROIs) were manually delineated layer by layer along the IPFP boundary on the vMRE maps until the entire IPFP region was encompassed, ensuring that any regions corresponding to cystic degenerations or fluid were excluded, as well as loose bodies. From the segmented IPFP regions, the mean vMRE stiffness (μ_{diff}) and the standard deviation (SD) of the mean were automatically extracted. Additionally, the distribution of vMRE stiffness values within the visualized IPFP region was automatically computed (Fig. 1). All images were independently assessed by two trained radiologists (N.Y. and Q.F. with 11 and 8 years of experience in musculoskeletal imaging, respectively). The radiologists were blinded to the patients' clinical data and spent approximately 5 min per individual assessment. Each subject was measured three times, and the average value was recorded. Both observers conducted the segmentation twice, with a 3-week interval to mitigate recall bias. The results from both observers were utilized to evaluate test-retest repeatability, as well as intra- and inter-observer agreement. Additionally, the knee K-L grade was determined by consensus of the two radiologists (Y.Y. and H.T. with 15 and 9 years of experience in musculoskeletal imaging, respectively) with reference to the atlas based on the Kellgren-Lawrence grading system.

Statistical analysis

SPSS 26.0 (IBM Corp., Armonk, NY, USA) and GraphPad Prism version 8.0 for Windows (GraphPad Software Inc., San Diego, CA, USA) were used for statistical analysis. The normality of continuous variables was evaluated using the Kolmogorov-Smirnov test. Data are presented as mean and standard deviations. The t-test was employed to determine whether stiffness values measured by μ_{diff_1500} differed from those measured by μ_{diff_800}. Inter- and intra-observer agreement was assessed by calculating the intraclass correlation coefficient (ICC) using two-way random model effects, with absolute agreement and average measurement, accompanied by a 95% confidence interval (CI). The following criteria were applied for analyzing the ICC: excellent (ICC ≥ 0.90), good (0.75 ≤ ICC < 0.90), moderate (0.50 ≤ ICC < 0.75), and poor (ICC < 0.50). Test-retest repeatability was evaluated by calculating the coefficient of variation (CoV%), which was computed as the percentage of the standard deviation (SD) of the mean (SD*100%/mean) derived from data obtained by observer 1 and observer 2 for each participant individually. The interpretation of CoV was performed as follows: excellent (CoV ≤ 10%), good (10%˂ CoV ≤ 20%), acceptable (20% ˂ CoV ≤ 30%), and poor (CoV > 30%). Furthermore, the Bland–Altman analysis was performed, which included scatterplots and Bland–Altman plots with 95% limits of agreement (LoA) and corresponding confidence intervals. The associations between vMRE measurements and K-L grade were assessed using Spearman's correlation coefficients. $P < 0.05$ was considered statistically significant.

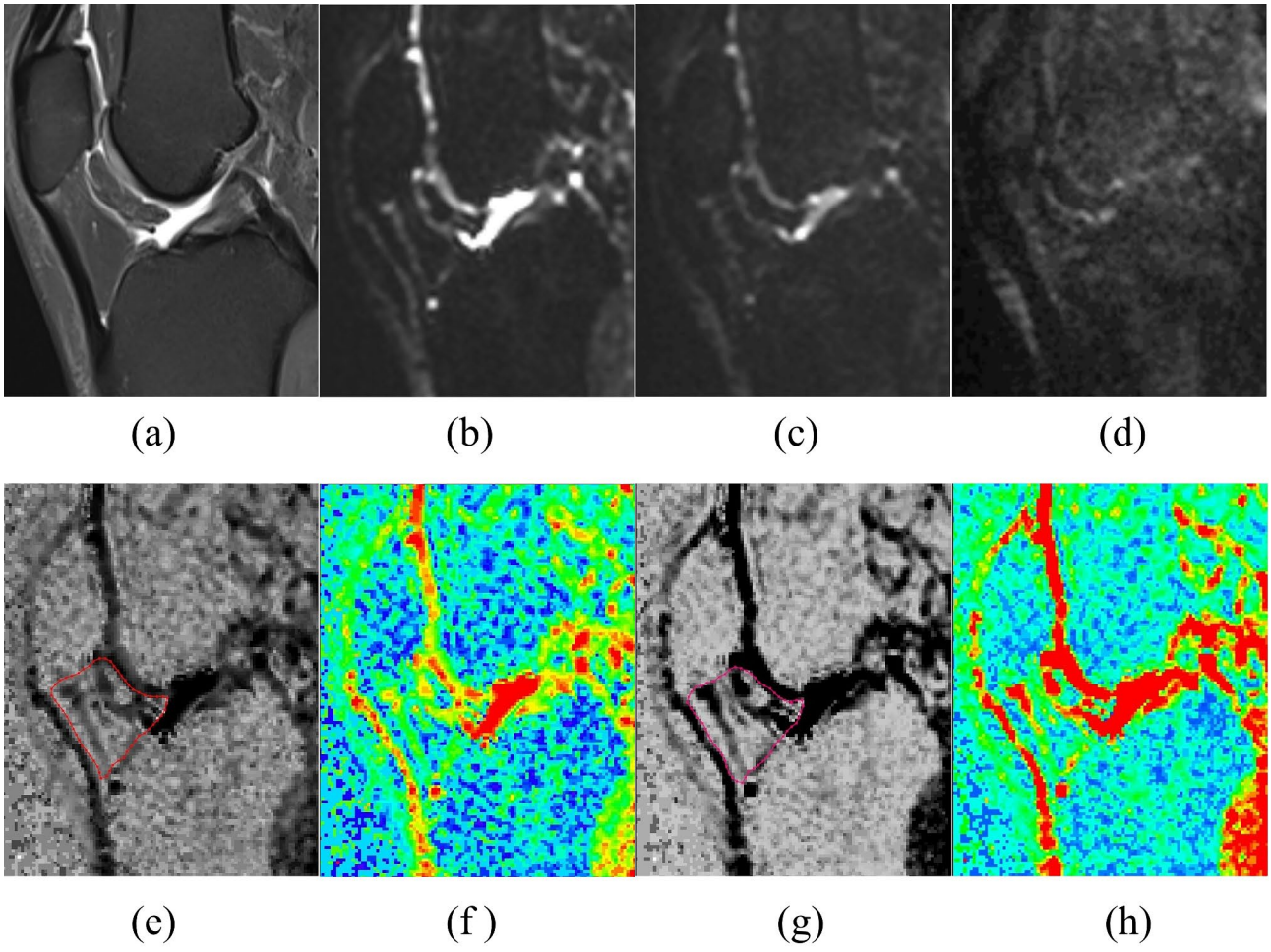

Fig. 1 A 52-year-old female with right knee joint, K-L grade 2. (**a**) represents the T2-weighted fat-suppressed image; (**b**), (**c**), and (**d**) illustrate the original images with b-values of 200, 800, and 1500 s/mm^2, respectively. (**e**) shows the virtual stiffness map of μ_{diff_800}, and (**f**) presents the corresponding pseudo-color map. (**g**) represents the virtual stiffness map of μ_{diff_1500}, and (**h**) provides the corresponding pseudo-color map. The region of interest (ROI) encompasses the area of the IPFP. The virtual stiffness values for μ_{diff_800} and μ_{diff_1500} are 11.72 kPa and 10.85 kPa, respectively

Table 1 Demographic characteristics of the subjects

Variable	Value ($n=71$)
Age (years), median (IQR)	56 (47.5, 68.6)
Males (%)	37 (52.1%)
Height (cm)	167.5 ± 8.9
Weight (kg)	69.6 ± 10.7
BMI (kg/m^2)	24.8 ± 3.5
Lateral (R/L, %)	39 (54.93%)/32 (45.07%)
Kellgren and Lawrence Grade	
Grade 0/1 (%)	23 (32.4%)
Grade 2 (%)	27 (38.0%)
Grade 3 (%)	21 (29.6%)

BMI body mass index, *IQR* interquartile range

Results

Patient characteristics

A total of 71 consecutive patients were included in the study (38 males and 33 females, median age 56 years, range 41– 72) with an average body mass index (BMI) of 24.8 ± 3.5 kg/m^2. The distribution of subjects by K/L grade was as follows: 23 in grade 0/1, 27 in grade 2, and 21 in grade 3. The characteristics of all participants are detailed in Table 1. The mean stiffness value measured on the vMRE maps was significantly higher for the μ_{diff_800} than the μ_{diff_1500} ($P<0.05$). Additionally, as the K/L grade increased, the stiffness values of the IPFP decreased for both μ_{diff_800} and μ_{diff_1500} ($P<0.05$). The stiffness values of the IPFP measured by two observers across two measurements (M_1 and M_2) are presented in Table 2.

Intra-observer reproducibility

The mean and SD values of μ_{diff_1500} demonstrated excellent intra-observer reproducibility with an ICC ≥ 0.90 and CoV ≤ 10% ($P^<$ 0.001). The ICCs for the mean and SD values of μ_{diff_800} were 0.901 and 0.870, respectively, although the CoV exceeded 10% ($P^<$ 0.001). For the mean values of μ_{diff_1500} and μ_{diff_800}, the mean bias (SD) between measurements conducted by the same observer

Table 2 Quantitative analysis of the stiffness values of IPFP between observer 1 and observer 2 in two measurements (M_1 and M_2)

	μ_{diff_1500} (kPa)				μ_{diff_800} (kPa)			
	Observer 1		Observer 2		Observer 1		Observer 2	
	M_1	M_2	M_1	M_2	M_1	M_2	M_1	M_2
Grade 0/1								
Mean	11.66 ± 0.73	11.93 ± 0.81	11.55 ± 0.78	11.66 ± 0.77	12.08 ± 0.58	12.48 ± 0.69	12.12 ± 0.55	12.43 ± 0.63
SD	4.44 ± 0.68	4.43 ± 0.62	4.42 ± 0.59	4.43 ± 0.60	4.00 ± 0.67	4.08 ± 0.69	3.82 ± 0.42	3.87 ± 0.43
Grade 2								
Mean	9.95 ± 0.46	9.89 ± 0.53	10.00 ± 0.59	9.96 ± 0.63	10.84 ± 0.46	11.13 ± 0.59	10.84 ± 0.50	10.74 ± 0.59
SD	5.20 ± 0.64	5.18 ± 0.65	5.15 ± 0.62	5.13 ± 0.66	4.42 ± 0.61	4.52 ± 0.58	4.38 ± 0.51	4.40 ± 0.51
Grade 3								
Mean	8.46 ± 1.28	8.24 ± 1.17	8.48 ± 1.22	8.45 ± 1.25	9.72 ± 0.92	9.46 ± 0.88	9.66 ± 0.87	9.74 ± 0.88
SD	5.40 ± 1.02	5.28 ± 0.61	5.52 ± 1.29	5.29 ± 0.72	4.65 ± 1.12	4.55 ± 0.91	4.77 ± 1.34	4.83 ± 1.06
Total								
Mean	10.07 ± 1.53	10.06 ± 1.69	10.05 ± 1.49	10.06 ± 1.55	10.91 ± 1.14	11.07 ± 1.39	10.90 ± 1.17	10.99 ± 1.28
SD	5.01 ± 0.87	4.97 ± 0.73	5.02 ± 0.96	4.95 ± 0.75	4.35 ± 0.84	4.39 ± 0.75	4.32 ± 0.90	4.35 ± 0.79

SD standard deviation

Table 3 Intra- and inter-observer reproducibility of μ_{diff} of the IPFP

	μ_{diff_1500}		μ_{diff_800}	
	Mean	SD	Mean	SD
Intra-observer Reproducibility				
ICC (95%CI)	0.968 (0.950, 0.980)	0.902 (0.848, 0.938)	0.917 (0.864, 0.946)	0.870 (0.800, 0.917)
CoV%	3.8	7.1	12.5	10.2
95% LoA	(-0.73, 0.76)	(-0.82, 0.79)	(-0.48, 0.50)	(-0.86, 0.92)
Bias (SD)	0.014 (0.38)	0.015 (0.41)	0.010 (0.25)	0.030 (0.44)
P	< 0.001	< 0.001	< 0.001	< 0.001
Inter-observer Reproducibility				
ICC (95%CI)	0.991 (0.986, 0.995)	0.957 (0.932, 0.973)	0.901 (0.855, 0.944)	0.863 (0.812, 0.907)
CoV%	2.0	4.0	11.6	15.1
95% LoA	(-0.42, 0.36)	(-0.47, 0.47)	(-0.32, 0.38)	(-0.51, 0.48)
Bias (SD)	-0.029 (0.20)	-0.0009 (0.24)	0.032 (0.16)	-0.018 (0.24)
P	< 0.001	< 0.001	< 0.001	< 0.001

SD standard deviation, *ICC* intraclass correlation coefficient, *CoV* coefficient of variation, *LoA* limit of agreement

were 0.014 (0.38) and 0.010 (0.25), respectively, with 95% LoA ranging from – 0.73 to 0.76 and – 0.48 to 0.50. Additionally, the mean bias (SD) and 95% LoA for the SD values of μ_{diff_1500} and μ_{diff_800}were 0.015 (0.41) and (-0.82, 0.79), 0.030 (0.44) and (-0.86, 0.92), respectively. A comprehensive overview of the intra-observer agreement and Bland–Altman analysis is presented in Table 3; Fig. 2.

Inter-observer reproducibility

Table 3; Fig. 3 show the inter-observer reproducibility agreement. Inter-observer reproducibility was excellent for the mean and SD values of μ_{diff_1500} and the mean values of μ_{diff_800} in the IPFP (all ICCs ≥ 0.90 and CoV < 10%, P < 0.001). However, the ICC for the SD value of μ_{diff_800} was < 0.90 (P < 0.001), and the CoV for the mean and SD values of μ_{diff_800} were 11.6 and 15.1 (10% < CoV ≤ 20%). For the mean value of μ_{diff_1500} and μ_{diff_800}, the mean bias (SD) between measurements performed by the two observers were – 0.029 (0.20) and 0.032 (0.16), with 95% LoA of -0.42 to 0.36 and – 0.32 to 0.38, respectively. Additionally, the mean bias (SD) and 95% LoA for the SD values of μ_{diff_1500} and μ_{diff_800} were – 0.0009 (0.24) and (-0.47, 0.47), -0.018 (0.24) and (-0.51, 0.48), respectively.

Test-retest repeatability

The comparison of analyses from the two scans revealed no significant differences in the mean and SD value of μ_{diff} measurements (all P > 0.05) (Table 4). The test-retest repeatability for the mean value of μ_{diff_1500} was excellent, with an ICC of 0.902 and a CoV of 6.8%. The mean value of μ_{diff_800} exhibited good repeatability, with an ICC of 0.877 and a CoV of 15.3%. Additionally, the SD values for μ_{diff_1500} and μ_{diff_800} showed good repeatability, with ICCs of 0.803 (CoV = 11.5%) and 0.796 (CoV = 13.5%), respectively. The mean bias (SD) between the two scans was – 0.042 (0.66) for the mean value of μ_{diff_1500} and 0.091 (0.59) for μ_{diff_800}, respectively. The 95% LoA were – 1.36 to 1.28 for μdiff_1500 and – 0.96 to 1.14 for μdiff_800. For the SD values of μ_{diff_1500} and μ_{diff_800}, the mean bias (SD) was 0.10 (0.53) and 0.06 (0.55), respectively. The 95% LoA

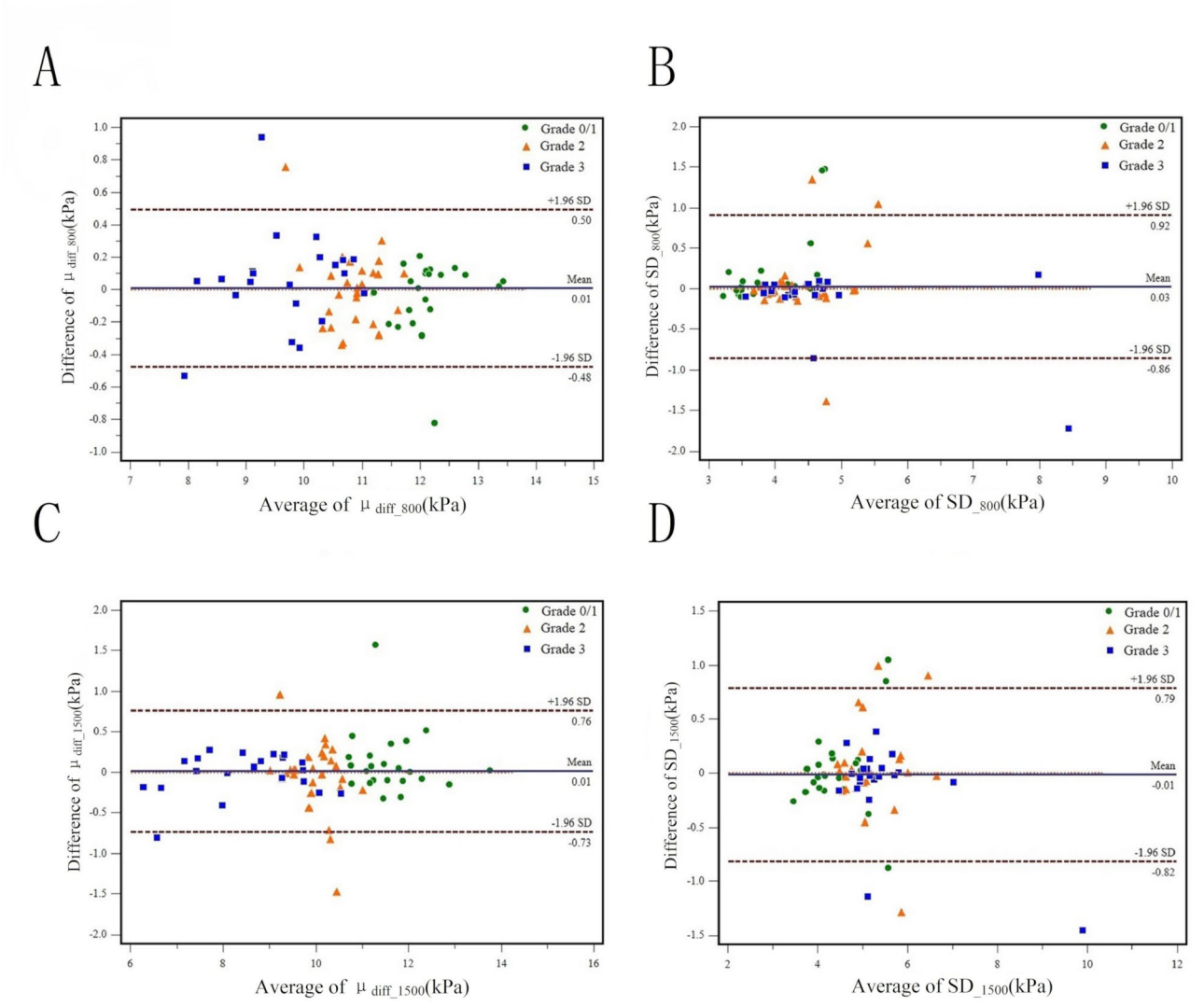

Fig. 2 Bland-Altman plots illustrating intra-observer reproducibility agreement of μ_{diff_800} (**a** and **b**) and μ_{diff_1500} (**c** and **d**). The x-axes represent the mean values of both measurements, and the y-axes depict the differences between M_1 and M_2. Blue line = mean absolute differences (bias). Dashed brown lines = 95% limits of agreement (LoA)

for μ_{diff_1500} ranged from − 1.26 to 1.06, while for μ_{diff_800}, it ranged from − 1.03 to 1.15. Corresponding Bland–Altman plots are presented in Fig. 4.

Correlation between vMRE measurements and K-L grade

Figure 5 presents a scatter plot between μdiff_1500, μdiff_800 and K-L grade. The μ_{diff} showed a negative correlation with the K-L grade ($r = -0.690$ for μ_{diff_1500}, and $r = -0.539$ for μ_{diff_800}, both $P < 0.001$).

Discussion

IVIM DWI-based virtual MRE is increasingly being investigated for application in body imaging. However, before wider clinical application of this technique can be recommended, technical parameters especially the repeatability and reproducibility of measurements need to be determined. In this study, the mean and standard deviation (SD) for the IPFP of μ_{diff_1500} and μ_{diff_800} measurements demonstrated excellent intra- and inter-observer reproducibility (ICCs > 0.9). Furthermore, the test-retest repeatability of μ_{diff_1500} also exhibited excellent reliability (ICC > 0.9), which was slightly higher than that of μ_{diff_800} (ICC < 0.9). To our knowledge, this is the first time to use this novel non-invasive method, namely vMRE, to verify its reproducibility and stability in the IPFP of knee joint.

Commonly employed non-invasive techniques for evaluating tissue stiffness in clinical practice include ultrasound elastography (USE) [24, 25] and MRE [26]. However, the major drawbacks of USE and MRE include high examination costs, the need for complex mechanical equipment, examiner dependency, and location of

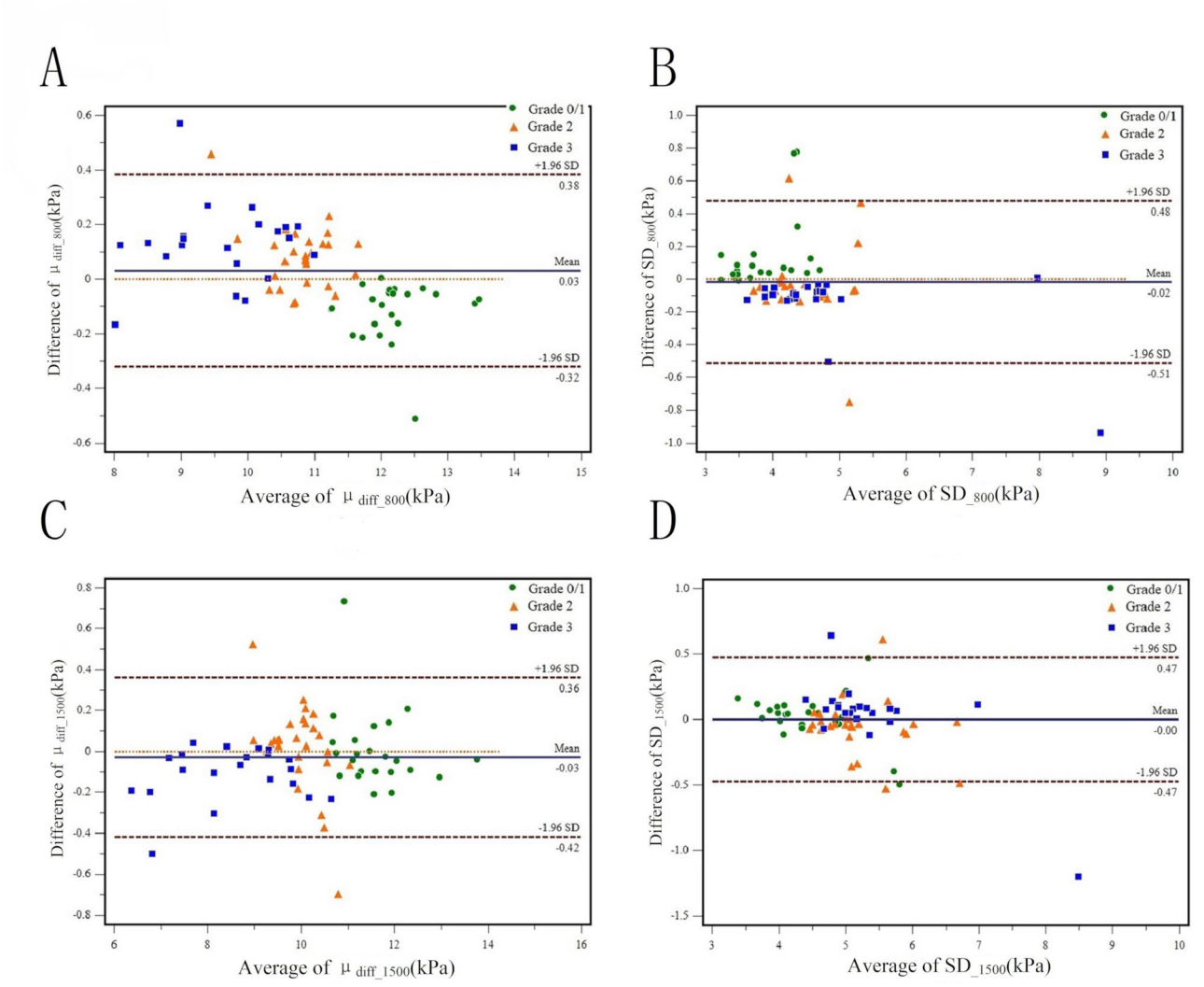

Fig. 3 Bland–Altman plots demonstrating inter-observer reproducibility of μ_{diff_800} (**a** and **b**) and μ_{diff_1500} (**c** and **d**) as assessed by observer 1 and observer 2. The x-axes show the mean values of both examinations, and the y-axes illustrate the differences between the two observers. Blue line = mean absolute differences (bias). Dashed brown lines = 95% limits of agreement (LoA)

Table 4 Test-retest repeatability of μ_{diff} of the IPFP

	μ_{diff_1500}		μ_{diff_800}	
	Mean	**SD**	**Mean**	**SD**
Test	10.07 ± 1.53	5.01 ± 0.87	10.91 ± 1.14	4.35 ± 0.84
Retest	10.12 ± 1.49	5.11 ± 1.03	10.81 ± 1.24	4.30 ± 0.91
t	-0.662	-1.339	1.539	0.827
P	0.510	0.185	0.128	0.411
ICC (95%CI)	0.902 (0.848,0.938)	0.803 (0.703,0.872)	0.877 (0.839,0.934)	0.796 (0.692,0.868)
CoV%	6.8	11.5	15.3	13.5
95% LoA	(-1.36, 1.28)	(-1.26,1.06)	(-0.96, 1.14)	(-1.03, 1.15)
Bias (SD)	-0.042 (0.66)	0.10 (0.53)	0.091 (0.59)	0.06 (0.55)

SD standard deviation, *ICC* intraclass correlation coefficient, *CoV* coefficient of variation; *LoA* limit of agreement

lesions. Recently, it has been proposed that tissue shear stiffness could be directly obtained from diffusion MRI without any mechanical vibration device [12, 27]. In this study, we generated two sets of μ_{diff} maps using the equation derived by Le Bihan et al., based on data obtained from two sets of b-values: 200–800 s/mm^2 and 200–1500 s/mm^2, respectively [23, 28]. The mean stiffness values obtained with μ_{Diff_1500} (10.07 ± 1.53 kPa) were

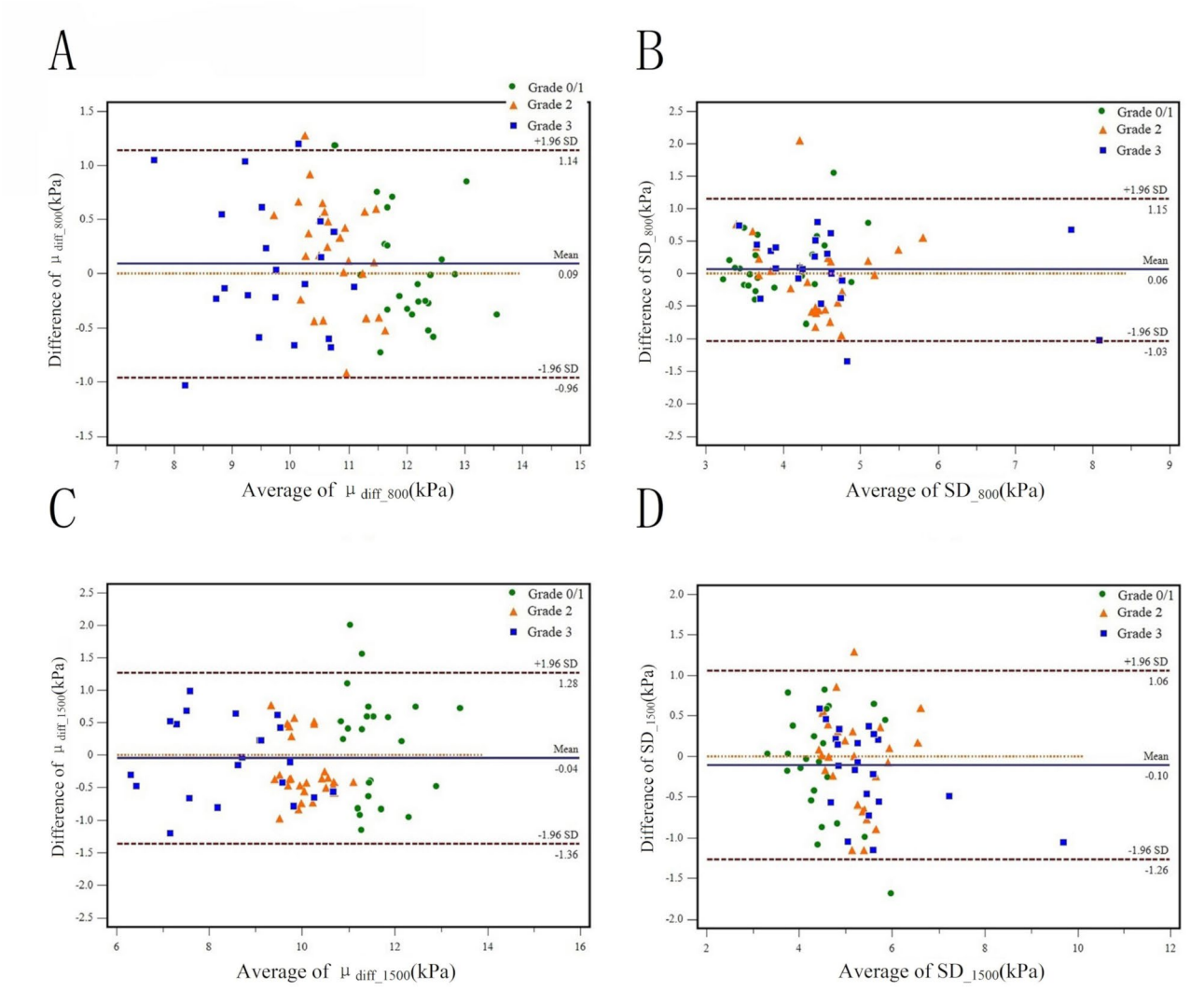

Fig. 4 Bland-Altman plots representing test-retest repeatability of μ_{diff_800} (**a** and **b**) and μ_{diff_1500} (**c** and **d**). The x-axes and y-axes reflect the mean values and differences between the two examinations, respectively. Blue line = mean absolute differences (bias). Dashed brown lines = 95% limits of agreement (LoA)

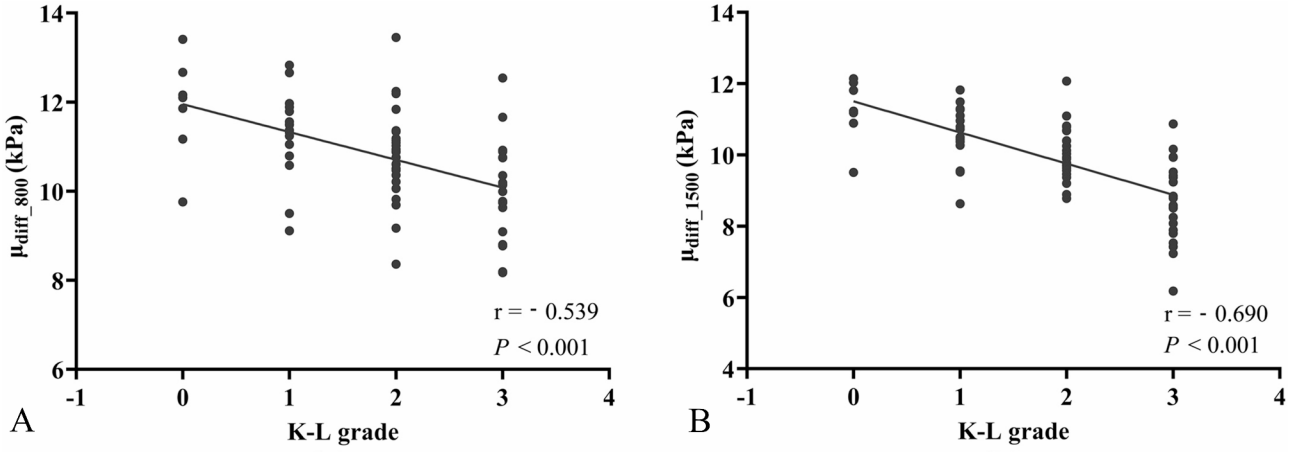

Fig. 5 Scatter plots showing the correlation of K-L grade with μ_{diff_800} (**a**) and μ_{diff_1500} (**b**)

lower than those with μ_{Diff_800} (10.91 ± 1.14 kPa). The degree of attenuation in IVIM images generates a novel type of contrast related to stiffness, which depends on tissue elasticity and the selection of acquisition parameters, primarily the IVIM b-value. In a previous study [29], fat-suppressed read-out segmented echo-planar imaging (rs-EPI) with multi-b-value DWI sequences was utilized to evaluate the stiffness between benign and malignant breast lesions, revealing a similar trend. Currently, there is no relevant research on KOA; however, it is impossible to fully assess the stiffness changes in the IPFP without MRE. It remains to be determined whether replicating the liver-based calibration factors proposed by Le Bihan in the IPFP would yield μ_{diff} values closer to those obtained with MRE [23]. Recent studies have demonstrated the potential applicability of the coefficients across different tissues. For instance, in research on placental vMRE, these coefficients were utilized to predict adverse outcomes in small - for-gestational-age infants [30]. In the field of oncology, studies on lung cancer and breast lesions have also applied these calibration coefficients in DWI - based vMRE [29, 31]. The results from these studies demonstrated the ability of these coefficients to differentiate between benign and malignant lesions, suggesting their effectiveness in tissues with diverse microstructures. However, we acknowledge that the IPFP is a distinct tissue, and there may be differences in its biomechanical properties compared to the liver and other tissues where these coefficients have been previously applied. Thus, our study represents an initial exploration in this area. Future research, particularly multicenter studies with larger sample sizes, is necessary to further validate and potentially optimize these coefficients specifically for the IPFP. We encourage other researchers to replicate our study and explore alternative calibration methods to improve the accuracy of elasticity measurements in the IPFP. Overall, while there is a need for caution, the existing applications in other organs give us confidence in the potential of these calibration coefficients for the IPFP, and we believe our study contributes to the growing body of knowledge in this field.

While the IPFP is primarily composed of adipose tissue, it also contains a significant amount of water, particularly in the context of inflammation and fibrosis. The use of fat-suppressed IVIM-DWI sequences in our study helps to minimize the confounding effects of fat signals, allowing for a more accurate assessment of water diffusion in the IPFP. Fibrosis in the IPFP is characterized by the excessive deposition of extracellular matrix (ECM) components, such as collagen, which can lead to changes in tissue microstructure. These structural changes may affect the diffusion of water molecules within the tissue. Specifically, increased collagen deposition can reduce the extracellular space and create barriers to water diffusion, leading to altered diffusion patterns that can be detected by IVIM-DWI. This hypothesis is supported by studies in other fibrotic tissues [32, 33].

We demonstrated good intra- and inter-observer reproducibility in the elasticity measurements in IPFP for both μ_{diff_1500} and μ_{diff_800} as indicated by high ICCs. These findings validated that the elasticity value can effectively represent the stiffness of the IPFP while being minimally influenced by measurement error. Consequently, these data suggest that the elasticity values derived from various combinations of b-values in IVIM-DWI may exhibit similarity in the IPFP. Several studies have explored the consistency and feasibility of employing virtual elastography in the assessment of meningiomas [34], pituitary adenomas [35], and breast lesions [29], yielding results consistent with all our findings. Notably, our research indicates that the reproducibility of μ_{diff_800} is somewhat inferior to that of μ_{diff_1500}. For μ_{diff_1500}, the mean and standard deviation demonstrated an ICC > 0.90 and a CoV of < 10%. In contrast, the ICC for the SD of μ_{diff_800} within and between observers < 0.90, with a CoV > 10%. It is well established that vMRE involves calculating the 'shifted' apparent diffusion coefficient (sADC) using DWI with b-values of 200 and 1500 s/mm^2. The corresponding calibration coefficients, α and β, were determined based on theoretical and experimental considerations; however, calibration coefficients for b-values of 200 and 800 s/mm^2 are currently unavailable, which may explain the slightly reduced consistency observed in the present study with μ_{diff_800}.

In this study, the short-term test-retest repeatability of IPFP elasticity was evaluated. The results indicated that the reproducibility of μ_{diff_1500} was excellent (ICC = 0.902, CoV = 6.8%, $P > 0.05$), while μ_{diff_800} demonstrated relatively poor reproducibility (ICC = 0.877, CoV = 15.3%, $P > 0.05$), which is consistent with findings from previous studies conducted on other organs [29, 30]. Although the detailed error values may differ to some extent, Rasmussen et al. investigated the brain tissue hardness of 32 healthy volunteers, finding the better reproducibility of DWI_{stiff_1000} than that of DWI_{stiff_1500} [28]. This discrepancy may stem from using a single index DWI model to scan two sets of b-value combinations separately, which is inconsistent with our study. Our study employed a dual index DWI model with a single scan encompassing 10 b-values. Previous research has demonstrated the clinical value of IVIM in identifying high signals within the IPFP [4]. Accordingly, we selected a low b-value of 200 s/mm^2 and a high b-value of 800 and 1500 s/mm^2 for virtual elastography fitting. These specific b-value selections were made to optimize sensitivity for Gaussian and non-Gaussian diffusion [12, 23]. Abnormal high signal intensity within the IPFP is a common KOA indicator, potentially due to fibrotic lesions [36, 37]. However,

in this study, we did not measure the elasticity value of the abnormally high signal area within the IPFP. It is well known that the range of high signal areas within the IPFP is typically small, and the variability of virtual elasticity values can be significantly influenced by the observers' experience, leading to measurement errors. Therefore, the region of interest (ROI) was delineated layer by layer across all IPFPs to minimize the impact of selection bias on the results.

In our study, as the K-L grade increased, the virtual stiffness values of the IPFP decreased. We found a significant negative correlation between the μ_{diff} values (both μ_{diff_1500} and μ_{diff_800}) and the K-L grade ($r = -0.690$ for μ_{diff_1500}, and $r = -0.539$ for μ_{diff_800}, both $P < 0.001$). This finding is consistent with the pathological changes observed in the IPFP throughout the progression of KOA. In the early stage of KOA (lower K - L grade), the fibrosis degree of the IPFP is relatively mild, maintaining a certain elasticity, and the μ_{diff} value is high. As the disease progresses to a higher K - L grade, the IPFP is infiltrated by immune cells, which secrete inflammatory mediators and trigger fibrosis, which is often accompanied by inflammatory infiltration, edema, and neovascularization. While fibrosis may locally stiffen collagen-rich regions, the overall IPFP microenvironment (e.g., edema-induced swelling) could dominate the diffusion signal, leading to a reduction in μ_{diff} despite the presence of fibrosis. This phenomenon aligns with study in other water-rich tissues [30]. This finding not only provides evidence for the potential of vMRE in evaluating the progression of KOA but also suggests that μ_{diff} values could serve as a potential quantitative biomarker for monitoring the disease. In a cross-sectional study conducted by Yoshinori Satake et al. [25], which involved 97 patients with KOA utilizing ultrasound elastography (USE), the findings revealed a significant correlation between the elasticity of the IPFP and anterior knee pain in these patients. This difference may arise from the distinct physical principles underlying USE and vMRE. USE reflects the mechanical properties at a macroscopic scale by measuring the shear wave speed (m/s). In contrast, vMRE indirectly derives elastic values from water diffusion characteristics, which are particularly sensitive to microstructural changes. Fibrosis diminishes the extracellular space and restricts water diffusion, leading to lower μ_{diff} values (kPa) observed in our study.

Although the results of this study are promising, several limitations warrant acknowledgment. Firstly, this prospective, single-center study requires further validation in a larger multicenter cohort. Secondly, there is currently no consensus on selecting b-values and calibration factors. Most research reports are based on Le Bihan's work regarding liver fibrosis; however, this study represents the first investigation of the IPFP in KOA. Consequently, we encourage other scholars to replicate our research. Additionally, the study emphasizes reproducibility rather than diagnostic accuracy. In our study, IPFP stiffness was assessed indirectly using the vMRE technique. While this method shows promising potential, it cannot fully substitute for direct measurement of actual IPFP stiffness. Future studies employing direct stiffness measurements are needed to further elucidate the relationship between IPFP mechanical properties and KOA progression, thereby providing more robust evidence to support the diagnosis and treatment monitoring of KOA. Lastly, the scanning time for IVIM in this study exceeded 6 min, which remains relatively lengthy for clinical practice. Therefore, further optimization of vMRE technology may be necessary to enhance its sensitivity and specificity.

Conclusions

The findings of this study suggest that vMRE is a reliable technique for assessing the elasticity of IPFP, demonstrating good intra-observer, inter-observer, and short-term retest consistencies. vMRE has the potential to act as a valuable tool for evaluating IPFP fibrosis in KOA and for monitoring disease progression and treatment response. Nevertheless, further research is required to validate the diagnostic accuracy of vMRE and to optimize the technique for clinical application.

Abbreviations

BMI	Body mass index
CoV	Coefficient of variation
FOV	Field-of-view
ICC	Intra-class correlation coefficient
IPFP	Infrapatellar fat pad
IVIM-DWI	Intravoxel incoherent motion diffusion-weighted imaging
K/L	Kellgren-Lawrence
KOA	Knee osteoarthritis
LoA	Limits of agreement
ROI	Region of interest
sADC	Shifted apparent diffusion coefficient
SD	Standard deviation
TR/TE	Repetition time/Echo time
USE	Ultrasound elastography
vMRE	Virtual magnetic resonance elastography

Acknowledgements

None.

Author contributions

Conception and design (HT, QF, NY, SG, YY); analysis and interpretation of the data (HT, QF, SG); drafting the article (HT, QF); critical revision of the article for important intellectual content (SG, SW, NY); and final approval of the article (HT, QF, YY, NY, SW, SG). All authors reviewed the manuscript.

Funding

This study was funded by the General Projects of Shaanxi Provincial Department of Science and Technology (No.2023-YBSF-020) and the Special Research Plan Projects of the Shaanxi Provincial Education Department (No. 22JK0356).

Data availability

No datasets were generated or analysed during the current study.

Declarations

Ethical approval and consent to participate

This study was approved by the Institutional Review Board of the affiliated hospital of Shaanxi University of Chinese Medicine (SZFYIEC-YJ-2024-47). All procedures were performed in accordance with the Declaration of Helsinki and relevant guidelines. All participants provided written informed consent to the protocol before the commencement of the study.

Consent for publication

Not applicable.

Competing interests

The authors declare no competing interests.

Clinical trial number

Not applicable.

Author details

[1]The First School of Clinical Medicine, Lanzhou University, Lanzhou 730000, Gansu, China
[2]Department of Radiology, The First Hospital of Lanzhou University, Lanzhou 73000, Gansu, China
[3]Department of Radiology, Affiliated Hospital of Shaanxi University of Chinese Medicine, Xianyang 712000, Shaanxi, China
[4]MR Senior Scientific Marketing Specialist, Siemens Healthineers, Shanghai, China

Received: 11 November 2024 / Accepted: 14 April 2025
Published online: 22 April 2025

References

1. Duong V, Oo WM, Ding C, Culvenor AG, Hunter DJ. Evaluation and treatment of knee pain: a review. JAMA. 2023;330(16):1568–80. https://doi.org/10.1001/jama.2023.19675
2. Zhu S, Wang Z, Liang Q, Zhang Y, Li S, Yang L, et al. Chinese guidelines for the rehabilitation treatment of knee osteoarthritis: an CSPMR evidence-based practice guideline. J evidence-based Med. 2023;16(3):376–93. https://doi.org/10.1111/jebm.12555
3. Zeng N, Yan ZP, Chen XY, Ni GX. Infrapatellar fat pad and knee osteoarthritis. Aging Disease. 2020;11(5):1317–28. https://doi.org/10.14336/ad.2019.1116
4. Tan H, Kang W, Fan Q, Wang B, Yu Y, Yu N, et al. Intravoxel incoherent motion diffusion-weighted MR imaging findings of infrapatellar fat pad signal abnormalities: comparison between symptomatic and asymptomatic knee osteoarthritis. Acad Radiol. 2023;30(7):1374–83. https://doi.org/10.1016/j.acra.2022.11.010
5. Ye Q, He D, Ding X, Wang Y, Wei Y, Liu J. Quantitative evaluation of the infrapatellar fat pad in knee osteoarthritis: MRI-based radiomic signature. BMC Musculoskelet Disord. 2023;24(1):326. https://doi.org/10.1186/s12891-023-06433-7
6. Zhong L, Li M, Du X, Ding Y, Zhang X, Mei Y, et al. Quantitative evaluation of the characteristic of infrapatellar fat pad fat content and unsaturation index by using hydrogen proton MR spectroscopy. Magn Reson Imaging. 2022;94:18–24. https://doi.org/10.1016/j.mri.2022.07.014
7. Cheung YY, Doyley M, Miller TB, Kennedy F, Lynch F Jr., Wrobel JS, et al. Magnetic resonance elastography of the plantar fat pads: preliminary study in diabetic patients and asymptomatic volunteers. J Comput Assist Tomogr. 2006;30(2):321–6. https://doi.org/10.1097/00004728-200603000-00031
8. Ehman RL. Magnetic resonance elastography: from invention to standard of care. Abdom Radiol (New York). 2022;47(9):3028–36. https://doi.org/10.1007/s00261-022-03597-z
9. Zerunian M, Masci B, Caruso D, Pucciarelli F, Polici M, Nardacci S, et al. Liver magnetic resonance elastography: focus on methodology, technique, and feasibility. Diagnostics (Basel Switzerland). 2024;14(4). https://doi.org/10.3390/diagnostics14040379
10. Yin M, Ehman RL. MR elastography: practical questions, from the AJR special series on imaging of fibrosis. AJR Am J Roentgenol. 2024;222(1):e2329437. https://doi.org/10.2214/ajr.23.29437
11. Ai Z, Han Q, Huang Z, Wu J, Xiang Z. The value of multiparametric histogram features based on intravoxel incoherent motion diffusion-weighted imaging (IVIM-DWI) for the differential diagnosis of liver lesions. Ann Transl Med. 2020;8(18):1128. https://doi.org/10.21037/atm-20-5109
12. Le Bihan D. What can we see with IVIM MRI? NeuroImage. 2019;187:56–67. https://doi.org/10.1016/j.neuroimage.2017.12.062
13. Kromrey ML, Le Bihan D, Ichikawa S, Motosugi U. Diffusion-weighted MRI-based virtual elastography for the assessment of liver fibrosis. Radiology. 2020;295(1):127–35. https://doi.org/10.1148/radiol.2020191498
14. Ioan-Facsinay A, Kloppenburg M. An emerging player in knee osteoarthritis: the infrapatellar fat pad. Arthritis Res Therapy. 2013;15(6):225. https://doi.org/10.1186/ar4422
15. Braun S, Zaucke F, Brenneis M, Rapp AE, Pollinger P, Sohn R, et al. The corpus adiposum infrapatellare (Hoffa's fat pad)-the role of the infrapatellar fat pad in osteoarthritis pathogenesis. Biomedicines. 2022;10(5). https://doi.org/10.3390/biomedicines10051071
16. Draghi F, Ferrozzi G, Urciuoli L, Bortolotto C, Bianchi S. Hoffa's fat pad abnormalities, knee pain and magnetic resonance imaging in daily practice. Insights Imaging. 2016;7(3):373–83. https://doi.org/10.1007/s13244-016-0483-8
17. Ballegaard C, Riis RG, Bliddal H, Christensen R, Henriksen M, Bartels EM, et al. Knee pain and inflammation in the infrapatellar fat pad estimated by conventional and dynamic contrast-enhanced magnetic resonance imaging in obese patients with osteoarthritis: a cross-sectional study. Osteoarthritis Cartilage. 2014;22(7):933–40. https://doi.org/10.1016/j.joca.2014.04.018
18. Emmi A, Stocco E, Boscolo-Berto R, Contran M, Belluzzi E, Favero M, et al. Infrapatellar fat pad-synovial membrane anatomo-fuctional unit: microscopic basis for Piezo1/2 mechanosensors involvement in osteoarthritis pain. Front Cell Dev Biol. 2022;10:886604. https://doi.org/10.3389/fcell.2022.886604
19. Onuma H, Tsuji K, Hoshino T, Inomata K, Udo M, Nakagawa Y, et al. Fibrotic changes in the infrapatellar fat pad induce new vessel formation and sensory nerve fiber endings that associate prolonged pain. J Orthop Res. 2020;38(6):1296–306. https://doi.org/10.1002/jor.24580
20. Hanniman E, Costa AF, Bowen CV, Abdolell M, Stueck A, McLeod M, et al. Prospective evaluation of virtual MR elastography with diffusion-weighted imaging in subjects with nonalcoholic fatty liver disease. J Magn Reson Imaging: JMRI. 2022;56(5):1448–56. https://doi.org/10.1002/jmri.28154
21. Jung HN, Ryoo I, Suh S, Lee YH, Kim E. Evaluating the elasticity of metastatic cervical lymph nodes in head and neck squamous cell carcinoma patients using DWI-based virtual MR elastography. Magn Reson Med Sciences: MRMS: Official J Japan Soc Magn Reson Med. 2024;23(1):49–55. https://doi.org/10.2463/mrms.mp.2022-0082
22. Zhang W, Doherty M, Peat G, Bierma-Zeinstra MA, Arden NK, Bresnihan B, et al. EULAR evidence-based recommendations for the diagnosis of knee osteoarthritis. Ann Rheum Dis. 2010;69(3):483–9. https://doi.org/10.1136/ard.2009.113100
23. Le Bihan D, Ichikawa S, Motosugi U. Diffusion and intravoxel incoherent motion MR imaging-based virtual elastography: a hypothesis-generating study in the liver. Radiology. 2017;285(2):609–19. https://doi.org/10.1148/radiol.2017170025
24. Ferraioli G, Barr RG, Berzigotti A, Sporea I, Wong VW, Reiberger T, et al. WFUMB guideline/guidance on liver multiparametric ultrasound: part 1. Update to 2018 guidelines on liver ultrasound elastography. Ultrasound Med Biol. 2024;50(8):1071–87. https://doi.org/10.1016/j.ultrasmedbio.2024.03.013
25. Satake Y, Izumi M, Aso K, Ikeuchi M. Association between infrapatellar fat pad ultrasound elasticity and anterior knee pain in patients with knee osteoarthritis. Sci Rep. 2023;13(1):20103. https://doi.org/10.1038/s41598-023-47459-0
26. Zhang YN, Fowler KJ, Ozturk A, Potu CK, Louie AL, Montes V, et al. Liver fibrosis imaging: a clinical review of ultrasound and magnetic resonance elastography. J Magn Reson Imaging: JMRI. 2020;51(1):25–42. https://doi.org/10.1002/jmri.26716
27. Jung HN, Ryoo I, Suh S, Kim B, You SH, Kim E. Differentiation of salivary gland tumours using diffusion-weighted image-based virtual MR elastography: a pilot study. Dento Maxillo Fac Radiol. 2024;53(4):248–56. https://doi.org/10.1093/dmfr/twae010
28. Rasmussen AM, Friismose AI, Mussmann B, Lagerstrand K, Harbo FSG, Jensen J. Repeatability of diffusion-based stiffness prediction - a healthy volunteer study. Radiography (London, England: 1995). 2024;30(2):524–530. https://doi.org/10.1016/j.radi.2024.01.008
29. Sun K, Zhu Y, Chai W, Zhu H, Fu C, Zhan W, et al. Diffusion-weighted MRI-based virtual elastography and shear-wave elastography for the assessment of breast lesions. J Magn Reson Imaging. 2024. https://doi.org/10.1002/jmri.29302

30. Deng J, Cao Y, Lu Y, Song J, Zhang A, Zhao M, et al. Value of placental virtual magnetic resonance elastography and intravoxel incoherent motion-based diffusion and perfusion in predicting adverse outcomes of small-for-gestational-age infants. Insights Imaging. 2023;14(1):153. https://doi.org/10.1186/s13244-023-01503-9
31. Zhang S, Du Y, Liang T, Zhang X, Guo Y, Yang J, et al. Diagnostic efficiency of intravoxel incoherent motion-based virtual magnetic resonance elastography in pulmonary neoplasms. Cancer Imaging. 2024;24(1):88. https://doi.org/10.1186/s40644-024-00728-1
32. Zhu J, Chen A, Gao J, Zou M, Du J, Wu PY, et al. Diffusion-weighted, intravoxel incoherent motion, and diffusion kurtosis tensor MR imaging in chronic kidney diseases: correlations with histology. Magn Reson Imaging. 2024;106:1–7. https://doi.org/10.1016/j.mri.2023.07.002
33. Chan HF, Weatherley ND, Johns CS, Stewart NJ, Collier GJ, Bianchi SM, et al. Airway microstructure in idiopathic pulmonary fibrosis: assessment at hyperpolarized (3)He diffusion-weighted MRI. Radiology. 2019;291(1):223–9. https://doi.org/10.1148/radiol.2019181714
34. Aunan-Diop JS, Andersen MCS, Friismose AI, Halle B, Pedersen CB, Mussmann B, et al. Virtual magnetic resonance elastography predicts the intraoperative consistency of meningiomas. J Neuroradiol. 2023;50(4):396–401. https://doi.org/10.1016/j.neurad.2022.10.006
35. Lagerstrand K, Gaedes N, Eriksson S, Farahmand D, De Coursey E, Johansson G, et al. Virtual magnetic resonance elastography has the feasibility to evaluate preoperative pituitary adenoma consistency. Pituitary. 2021;24(4):530–41. https://doi.org/10.1007/s11102-021-01129-4
36. Cen H, Yan Q, Han W, Meng T, Chen Z, Ruan G, et al. Longitudinal association of infrapatellar fat pad signal intensity alteration with biochemical biomarkers in knee osteoarthritis. Rheumatology (Oxford). 2022;62(1):439–49. https://doi.org/10.1093/rheumatology/keac214
37. Chang J, Liao Z, Lu M, Meng T, Han W, Ding C. Systemic and local adipose tissue in knee osteoarthritis. Osteoarthr Cartil. 2018;26(7):864–71. https://doi.org/10.1016/j.joca.2018.03.004

Publisher's note